Research Article

Weina Guo, Yantao Gao* and Lijuan Sun

In-situ CT characterization of 2D woven SiC_f/SiC composite loading under compression

https://doi.org/10.1515/secm-2022-0166
received May 16, 2022; accepted October 20, 2022

Abstract: SiC fiber-reinforced SiC matrix composites (SiC_f/SiC) with 2D woven fabric as preform were tested under compression with *in-situ* X-ray computed tomography. The microstructure and damage evolution of the material under continuous loading levels were accurately revealed by image reconstruction of CT data. There were inhomogeneous pores in SiC_f/SiC composite because of the uniform fiber distribution in the preform. The result also showed that 2D woven SiC_f/SiC composite had obvious non-linear characteristics by its compressive load–displacement curve, and the damage modes included transverse matrix cracking, interlayer cracking, longitudinal matrix cracking, and fiber bundle fracture. Matrix cracking tended to occur near the pores or holes of the material, and the number of longitudinal cracks was relatively high compared to the number of transverse cracks.

Keywords: SiC_f/SiC composite, *in-situ* CT, microstructure, damage evolution

1 Introduction

SiC_f/SiC composites are attractive for high-performance engineering applications due to their thermal properties, corrosion resistance, low density compared to metals, and higher toughness compared to monolithic ceramics [1–3]. Therefore, a thorough understanding of the complex damage initiation and accumulation mechanisms under typical mechanical loading conditions is essential for the safe design and practical service life prediction of SiC_f/SiC composites [4,5]. One-dimensional statistical models based on matrix and fiber failure probability laws (e.g., Weibull's law) have been well documented [6–13]. These models can make satisfactory predictions of macroscopic responses. However, they cannot be adequately validated for microscopic phenomena. In fact, even when qualitative damage evolution is accepted, most of the observations reported in the literature were confined to the surface and collected after the final failure, which does not facilitate the study of their damage process [14,15].

In-situ X-ray computed tomography (XCT) is a nondestructive testing technique developed in recent years, which enables 3D microscopic imaging of materials and can provide volumetric information about microstructure and microcrack meshes [16–18], which cannot be done by traditional microscopy techniques. Currently, some scholars [19,20] have successfully applied XCT techniques to the study of fracture failure processes of SiC_f/SiC and C_f/SiC composites and comprehensively analyzed the damage processes of a variety of composites under stress loading from microstructure analysis (Table 1). Zhang et al. [21] used XCT to study the plain SiC fiber-reinforced SiC matrix composites in terms of microstructure and tensile damage evolution and developed a miniature high-precision *in-situ* XCT test fixture that can be used to perform miniature XCT *in-situ* tensile tests. Ai et al. [22] reconstructed the precise microstructure of C_f/SiC composites composed of C fiber bundles and chemical vapor infiltration (CVI)–SiC matrix, performed *in-situ* tensile experiments on C_f/SiC composites using a CT real-time quantitative imaging system, and investigated the damage and failure characteristics of the material, which showed that the material damage occurred first at the defects and then extended to the fiber bundle SiC matrix interface, eventually forming macroscopic cracks. Duan et al. [23] investigated the bending progressive damage behavior of 2.5D SiC_f/SiC braided composites using a three-point bending method. In this process, acoustic emission and digital image correlation were used to monitor the damage progression. Subsequently, micro-CT was used to identify the internal damage evolution. It can be seen that the use of *in-situ* loaded CT imaging technique to study the

* **Corresponding author: Yantao Gao,** School of Textiles and Fashion, Shanghai University of Engineering Science, Shanghai 201620, China, e-mail: gaoyantao@sues.edu.cn
Weina Guo: School of Textiles and Fashion, Shanghai University of Engineering Science, Shanghai 201620, China
Lijuan Sun: The State Key Laboratory of Nonlinear Mechanics, Institute of Mechanics, Chinese Academy of Sciences, Beijing, China

Table 1: Examples of XCT technology applied to composites

Composite name	Research objective	Research method	Research results
C/SiC [19]	Tensile dynamic fracture	XCT Split Hopkinson pressure bar	Tensile failure: Delamination Fiber pullout Bundle breaking
SiC/SiC [20]	Tensile test Matrix crack propagation Fiber breaking occurrences	XCT Six successive loading levels	A slow and discontinuous propagation of matrix cracks, even after the occurrence of matrix crack saturation. Observations before the ultimate failure revealed only a few fibers breaking homogeneously along the minicomposite.
SiC/SiC [21]	Tensile damage evolution Microstructures	XCT Six successive loading levels High-precision *in-situ* XCT test fixture	Tensile failure: Transverse matrix cracking Longitudinal matrix cracking Fiber pull-outs
C/SiC [22]	*In-situ* tensile test Meso-structural Damage evolution Fracture behaviors	X-ray microtomography digital images Finite element analysis	Material damage initially occurs at the defects, followed by propagating toward the fiber-tow/SiC–matrix interfaces, ultimately, combined into macro-cracks
SiC/SiC [23]	Flexural progressive damage	XCT Acoustic emission Digital image correlation Three points bending method	2.5D warp samples present the pseudo-ductile fracture, whereas 2.5D weft samples indicate the brittle fracture
SiC/SiC [24]	Tensile test Failure events	XCT Finite element analysis	Stress concentrations in the planes containing the weft tows The first cracks and subsequent damage localization were found

damage failure mechanism of SiC_f/SiC composites has unique advantages [24].

However, most of the *in-situ* studies on the damage evolution of SiC_f/SiC composites have focused on tensile damage evolution [21,25,26], while the damage process of SiC_f/SiC composites under compression loading has rarely been reported. Therefore, in this article, for the damage evolution mechanism of plain SiC_f/SiC composites, *in-situ* XCT compression tests were carried out to investigate the damage process under transverse compression loading, the damage sprouting and evolution law of SiC_f/SiC composites during compression was revealed and failure behavior was analyzed.

2 Experimental

2.1 Description of SiC_f/SiC composites

The specimen was fabricated by CVI process, and the toughened phase was laminated 2D plain fabric woven by third-generation SiC fiber with about 500 fibers per fiber bundle and the average diameter of single fiber was 12.6 μm. Prior to CVI process, pyrolytic carbon was deposited on the preforms by chemical vapor deposition, yielding a thickness of about 200 nm. Methyltrichlorosilane was used to deposit the SiC matrix at 1,100°C until the density of composites remained steady. Specimens with a size of 2 mm × 4 mm × 20 mm were prepared for the test.

2.2 X-ray *in-situ* compression test

The laboratory-based interrupted *in-situ* CT imaging (described as in Figure 1) was performed under compression load in The State Key Laboratory of Nonlinear Mechanics, Institute of Mechanics, Chinese Academy of Sciences. The *in-situ* compression test equipment is the Y.CT Modular from Yxlon, Germany. A pause of about 20 min after every loading was needed for collecting tomogram at the related stress level. In the experiments, total ten loadings were conducted until final fracture. The compression force was successively loaded up to 483.657, 1288.506, 2330.982,

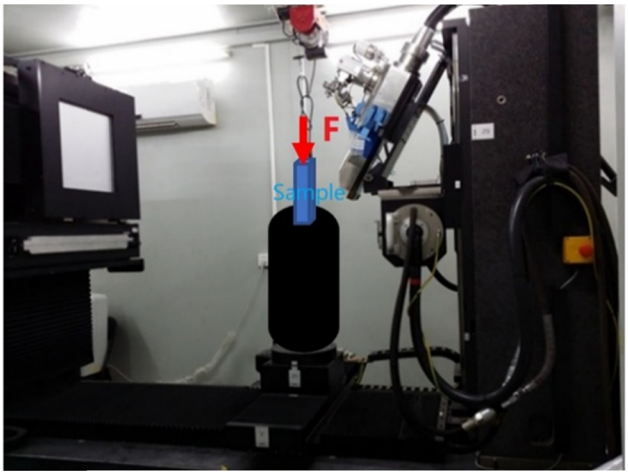

Figure 1: *In-situ* CT compression experiment.

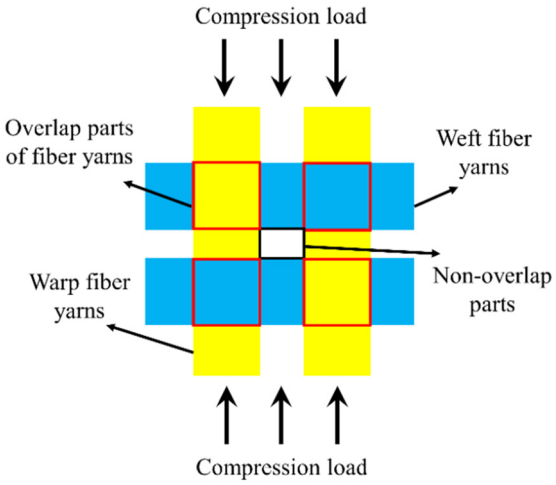

Figure 2: Structure of plain fabric.

2920.614, 3561.132, 4030.783, 3956.554, 3210.061, and 3262.348 N. As the requirement of sample size, the resolution of CT imaging used was selected as 9 μm.

3 Results and discussion

3.1 Analysis of initial microstructure

The complexity of the woven structure and CVI process will lead to defects such as pores in the woven SiC_f/SiC composites. First, 3D images reconstructed by CT data were used to detect the initial microstructure of SiC_f/SiC composites.

3.1.1 Initial defects

Pores are one of the major defects of SiC_f/SiC composites. The pores have a negative effect on the mechanical properties of the composite such as interlaminar shear strength, longitudinal and transverse bending strength, and longitudinal and transverse compression strength. Figure 2 shows the structure of the plain fabric. It can be seen that the four adjacent yarns do not closely overlap. The non-overlapping parts then form corresponding pores. The internal pores of the material can be divided into initial pores generated during the preparation process and damage cracks caused by external loading. The initial pores generated by SiC_f/SiC composites are a typical feature of the plain structure and the CVI densification process and can be distinguished in the reconstructed images. Depending on the volume of the pore structure, there are two types of initial pores, namely matrix micropores within the fiber bundles and macropores between the fiber bundles, as shown in Figure 3 [27].

From Figure 3, it can also be seen that the micropores in 2D woven SiC_f/SiC composites were mainly distributed inside the fiber bundles. By observing the pores in the fiber bundles, it was found that the micropores were distributed along the longitudinal direction of the fiber bundles. The micropores were small but large in number. Besides, there was almost no connection among the micropores. As shown in Figure 3, the large pores were mainly distributed in the non-overlapping areas of warp and weft yarns of each layer. This was because during the CVI process, the overlapping fiber yarns provided a larger surface area than the non-overlapping fiber yarns, and the matrix can be deposited rapidly in the fiber yarns. As the deposition process proceeded, the transport channels for the reaction gases gradually closed, eventually leading to the formation of large pores with low deposition rates in the non-overlapping areas. Overall, the distribution of both microporosity and large pores was irregular, but they can be clearly distinguished.

By applying threshold segmentation, variation of the porosity distribution on the slices in different directions can be clearly observed, as shown in Figure 4. From Figure 4, it can be observed that the distribution of porosity along different directional slices was not regular. In the *X* and *Y* directions, the surface fraction of porosity showed a complex variation due to the periodicity of the weaving pattern and the superimposed effect of the number of layers. This variation was due to the presence of an offset ("U") of the weft yarns in the *X*-direction, while the warp yarns were aligned with each other in

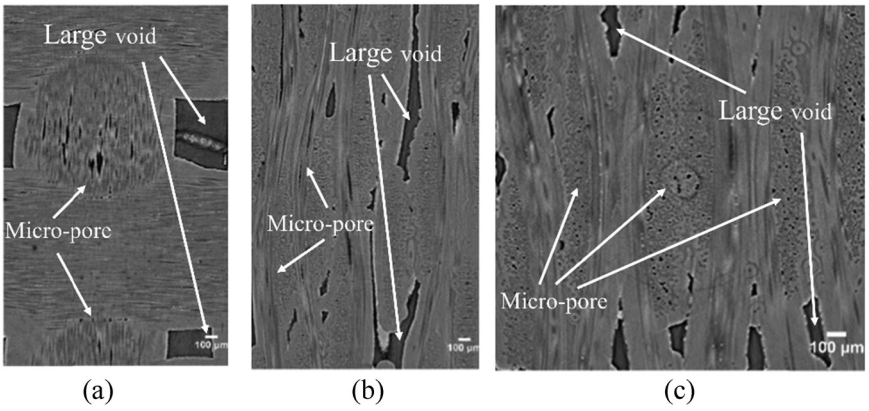

Figure 3: Distribution of initial holes on different slices: (a) XOY slice, (b) XOZ slice, and (c) YOZ slice [27].

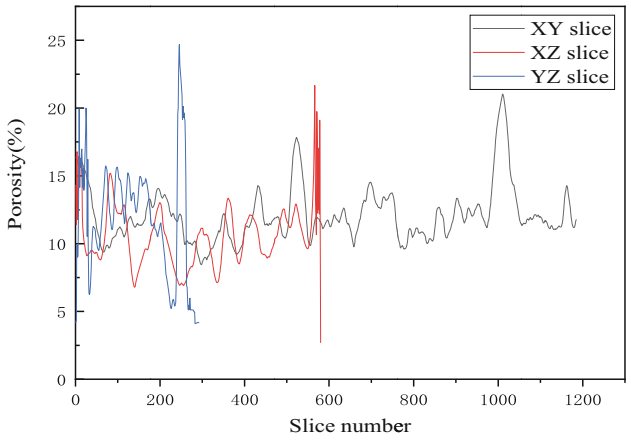

Figure 4: Porosity distribution of slices in three different directions.

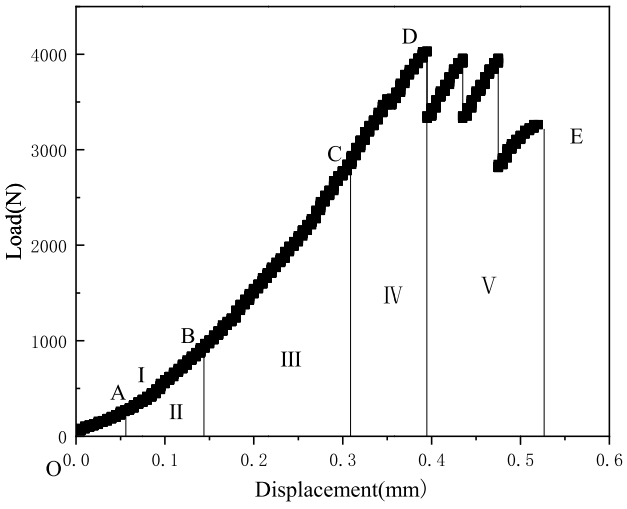

Figure 5: Compressive load–displacement curve of SiC_f/SiC composite.

the *Y*-direction. The porosity of the composite showed significant fluctuations in the *X* and *Y* directions due to the low porosity within the plies and the high porosity between the plies. The fluctuations in the *Z*-direction were related to the superposition of the plies in the composite. The local minima of porosity were caused by the intermediate planes within the layers and the maxima of porosity were related to the median plane between the two layers. Similar results were also found by Gelebart et al. [28] for the characterization of porosity of CVI SiC_f/SiC composites by X-ray chromatography.

3.2 Compression test results analysis

3.2.1 Load–displacement curve

The load–displacement response of the material during loading was a macroscopic characterization of its internal damage evolution process, and Figure 5 shows the load–displacement curve at successive loading levels. From this, the curve of the sample can be divided into five stages. The first stage (OA stage): at the beginning of loading, the curve was linear, and the sample load–displacement curve increased linearly along the straight line OA, indicating that the material was in the elastic deformation stage and almost no damage occurred, and the specimen can return to its original state after unloading. The second stage (AB stage): the curve showed a non-linear change, which might be caused by the gradual internal damage and the transmission of cracks along the matrix to the fibers and between the fiber layers. The third stage (BC stage): the curve shows linearity, and the displacement gradually increases with the increase of load. At this time, the cracks on the matrix gradually extend to the fiber–matrix bonding interface (i.e., the interface layer) with the increase in load, and the interface layer, as the bridge

connecting the matrix and the fiber inside the SiC_f/SiC composite, was the key factor regulating the bonding strength between the fiber and the matrix. Its components and structure largely determined the mechanical properties of SiC_f/SiC composites. The fourth stage (CD stage): as the load continued to increase, the slope of the curve gradually decreases. This indicates that the matrix has failed, and the stress-relieving effect of the interfacial layer has reached saturation, and cracks gradually start to sprout and expand inside the fibers. The fifth stage (DE stage): the curve was sawtooth-shaped, indicating that the matrix did not reach the ultimate load immediately after fracture, but after a "buffer period," which was because when the load reached the matrix critical load, crack expansion, interface debonding, fiber pullout and fracture, and other toughening effect absorb part of the stress. At the same time, the stresses were released by a small mutual "slip" between the matrix grains, so that the specimen can continue to withstand the load until the final fracture.

In addition, it can be observed from Figure 5 that the whole evolution of the load–displacement curve of the sample showed brittle fracture characteristics, which was due to the fact that the matrix was mainly loaded during compression, thus the load increased more slowly with displacement during the elastic deformation phase, and the material has a lower modulus of elasticity in parallel compression, and once the ultimate load that the matrix can withstand was exceeded, the matrix fractures or crushes and the curve drops steeply, leading to the destruction of the material.

3.2.2 Damage evolution process

The 3D reconstructed CT data under different loading states (the state 2: 483.657 N, the state 5: 2920.614 N, the state 8: 3956.54 N, and the state 10: 3262.348 N) were selected to visualize and analyze the microstructure morphology of the material during the compression process by using software "AVIZO 9.1" to observe the damage change information such as internal pore distribution, crack initiation, and size change of the material during the compression process.

The internal damage process of SiC_f/SiC composites during compression was obtained by observing the internal tomography of the material perpendicular to the three coordinate axes. Figure 6 shows a set of local CT 2D sections on the frontal ZOY section of the test piece. In the first loading condition, no damage was observed within the fiber matrix. In the fourth loading condition, there were two transverse cracks perpendicular to the compression direction. The crack indicated by the arrow in A occurs at the fiber bundle lap boundary, which was connected to the large hole and belonged to the matrix crack outside the fiber bundle. And the crack with the B arrow was a transverse crack of the matrix inside the weft fiber bundle. Longitudinal cracking parallel to the fiber direction occurs at loading condition 7, which started at the edge of the large matrix hole and extended inside the fiber bundle, and this longitudinal cracking was also observed in the cross-section at other locations inside the test piece. The longitudinal crack extension path related to the cracks at positions A and B (described in Figure 6) led to the fracture of the fiber bundle surrounded by the transverse and longitudinal cracks. Under the tenth loading condition, the test piece was already partially crushed, the longitudinal crack did not occur too close and the hole at the fracture of the fiber bundle became larger.

Figure 7 shows a set of local CT 2D sections on the ZOX cross-section of the side of the test piece. At the seventh loading, the cracks inclined to the compression direction can be clearly seen. As described in the figure, the crack at position A started from the large hole in the matrix and it extended from the hole to the inside of the

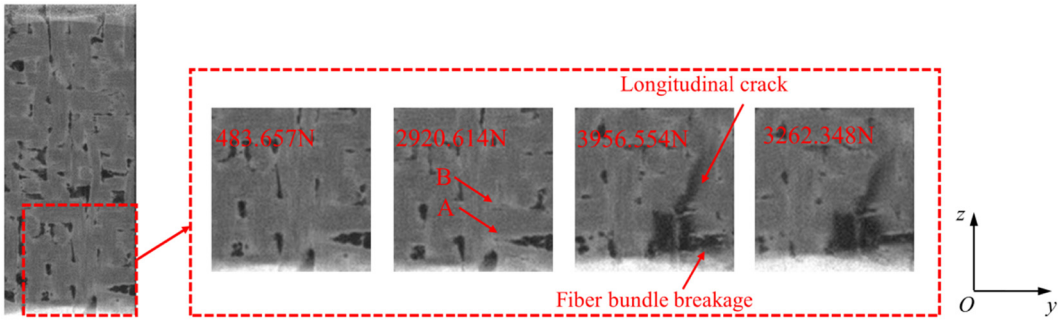

Figure 6: Damage evolution process of local area on ZOY cross-section.

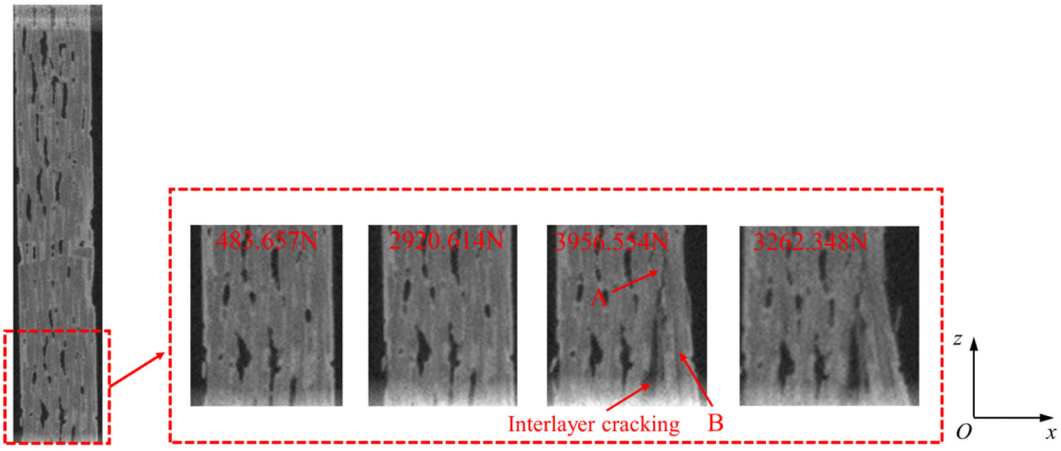

Figure 7: Damage evolution process of local area on ZOX cross-section.

fiber bundle and gradually parallel to the fiber bundle. The crack at B was a longitudinal crack inside the fiber bundle, which started from the edge of the test piece and extended to the inside of the test piece. In addition, a significant interlaminar cracking within the matrix between the two adjacent fiber bundles at the seventh loading condition was observed, where the cracking started from the hole, and the interlaminar cracking was almost parallel to the nearby fiber bundles. After the test piece was crushed, the interlaminar cracking was more pronounced and more longitudinal cracks appeared inside the fiber bundles than in the seventh loading condition.

Figure 8 shows a set of local CT 2D sections on the YOX cross-section of the test piece. No obvious changes were produced at the fourth loading, and there was a tendency for the local pores to shrink, and some of the micropores almost disappeared by the compression to the ninth loading. The cracks at positions A and B started from the holes and extended in a direction almost parallel to the weft fiber bundle, and the end of the cracks at position A extended to the beginning of the cracks at position B. The cracks at position B extended to the edge of the test piece and finally formed matrix cracks between the two layers, causing interlayer cracking. There were more voids, less matrix, and weaker interlayer connection at this place, so after the cracks sprouted under the seventh loading condition, the cracks gradually expanded as the pressure increased. By the ninth loading, the interlaminar cracking was so severe that the fiber bundles between the left and right of the interlaminar matrix separated.

Figure 9 shows the strain distribution calculated by digital volume correlation (DVC) under the maximum loading condition. Figure 9(a–c) shows the strains in the *X*, *Y*, and *Z* directions, respectively (*Z* direction is the loading direction). From the figures, the strain was not uniform, and the variation in the *Y* and *Z* directions was more serious than that in the *X* direction, and there was a serious strain concentration in the lower part of the test piece. Although the test piece was subjected to unidirectional compression load in the experiment, the internal stress state and deformation behavior were non-uniform and the complex stress/strain states due to the complexity of the material microstructure. The most severe deformation at the interlaminar crack can be observed in the lower part of the strain concentration, where one

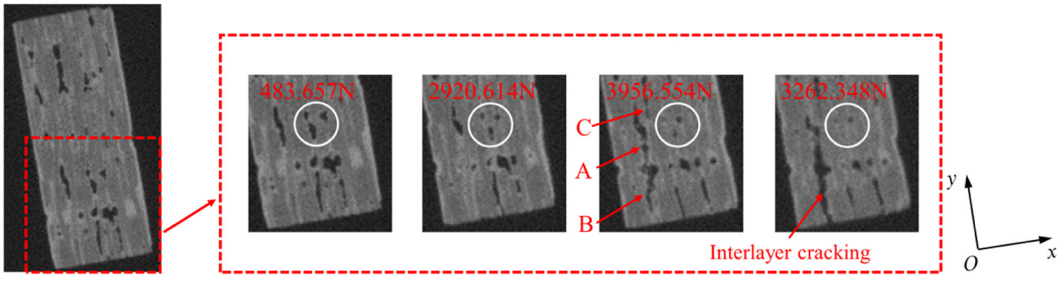

Figure 8: Damage evolution process of local area on YOX section.

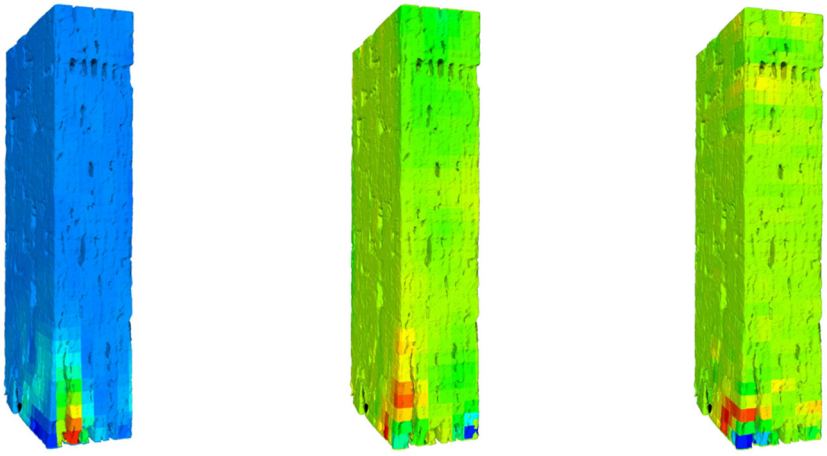

Figure 9: Strain distribution under maximum loading calculated by DVC: (a) *X*-direction, (b) *Y*-direction, and (c) *Z*-direction.

of the sides of the interlaminar crack moved outward, resulting in a significant change in its displacement in the *X*, *Y*, and *Z* directions, as shown in Figure 10. It was observed that the distribution of the displacement showed inhomogeneity, and its significant changes also occurred mainly in the stress concentration part. Therefore, the strain concentration had a significant effect on the displacement variation of the specimen.

3.2.3 Failure mechanisms

According to damage evolution of the material, it was found that the 2D woven SiC_f/SiC composites mainly experienced damage modes such as matrix transverse cracking, interlayer cracking, fiber bundle matrix longitudinal cracking, and fiber bundle fracture from the beginning of damage to final failure.

3.2.4 Transverse matrix cracking

Since the fracture strain of the matrix was small, transverse cracks in the matrix perpendicular to the compression direction occurred first during the compression process, which were mainly divided into transverse cracks in the matrix outside the fiber bundle and transverse cracks in the matrix inside the fiber bundle (Figure 6).

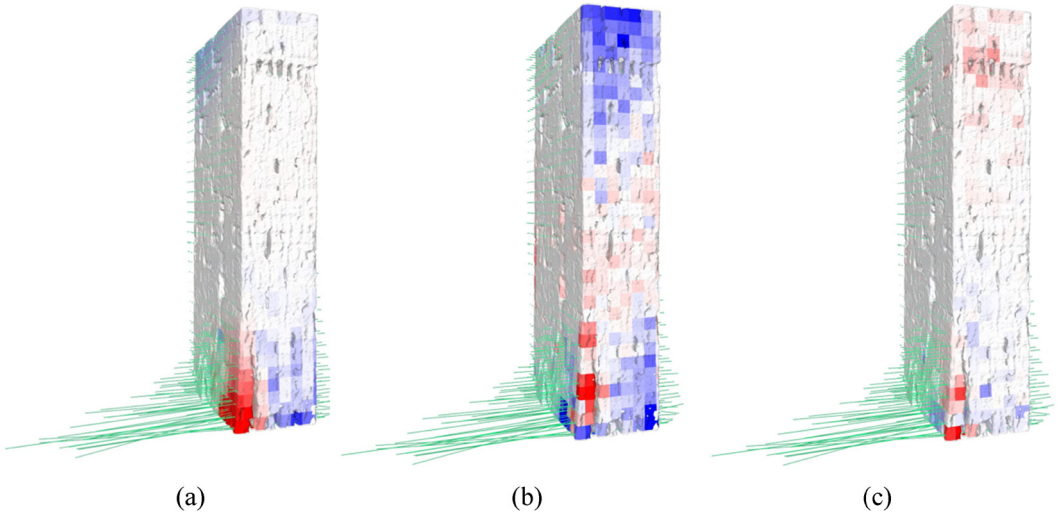

Figure 10: Displacement variation under maximum loading calculated by DVC: (a) *X*-direction, (b) *Y*-direction, and (c) *Z*-direction.

Matrix cracks in the fiber bundle mainly occurred in the weft direction, and many transverse cracks evolved from the development of microvoids in the fiber bundle. Due to the presence of a weak interfacial layer in the fiber, these transverse cracks generally extended along the interface and did not cause fiber fracture. Matrix cracks outside the fiber bundle mainly occurred at the fiber lap boundary, near the large holes in the matrix, and at the edges of the material, where the holes disrupted the continuity of the material and produced stress concentrations that promoted damage cracking.

3.2.5 Interlaminar cracking

As the loading increased, interlaminar cracking gradually appeared in the matrix between the bundles (Figure 7). Interlaminar cracking mostly sprouted at the edge of large holes and developed along the intersection of fiber bundles and the external matrix, and because the direction of interlaminar cracking was almost parallel to the adjacent fibers, it was not easy to enter the interior of fiber bundles in expansion, but was continuous within the matrix between the fiber layers, resulting in delamination of the material. In regions where interlaminar cracking was more severe, it can lead to separation of the interlaminar matrix from the fiber bundles on both the sides.

3.2.6 Longitudinal cracking of fiber bundles

The causes of longitudinal cracking inside the fiber bundles were more complex and were less likely to occur before material damage. The geometric characteristics of fiber bundles, their arrangement, and initial defects led to the susceptibility to stress concentration and longitudinal cracks along the ZOY plane inside the bundles (Figure 7); the fiber bundles were wavy, and the bundles were bent at the same time during the compression process, and the compression deformation of the upper and lower parts of the bundles was different in the longitudinal direction, which was prone to longitudinal cracks along the ZOX plane (Figure 6). It can be seen that when the compression load does not reach the strength limit of the composite, compression damage was resisted together by the fiber and matrix in the composite, and the damage modes were matrix cracking, delamination, and fiber bundle cracking.

3.2.7 Fiber bundle fracture

Fiber bundle fracture occurs as the composite reaches its strength limit, and the sudden release of the potential energy accumulated in the composite under compression causes a serious separation of the fiber bundle from the matrix. Thus, part of the fiber bundles fracture and cracks appear. When the fiber bundle breaks, the friction between the fiber bundle and the matrix can effectively absorb the energy generated by the compression load. At the same time, the fracture of the fiber bundle weakens the ability of the composite to resist damage. With the appearance of a large number of fiber fractures, composite loses the ability to continue to resist damage, and failure occurs finally.

4 Conclusion

In this article, we characterized the microstructure of 2D woven SiC_f/SiC composite using synchronous radiation X-ray computed tomography and investigated the damage evolution of the material under compression by *in-situ* CT experiment and discussed the damage evolution and failure mechanism of 2D woven SiC_f/SiC composites. The main conclusions are as follows:

(1) XCT can better reveal the microstructure, porosity distribution, and damage evolution of 2D SiC_f/SiC composite. The distribution of the initial porosity along the different directional slices has obvious irregularity. The micropores produced during the manufacturing process were small but large in number and distributed along the fiber bundles, and the large pores were mainly distributed in the overlapping areas of the warp and weft direction filament bundles.
(2) The load–displacement curves of SiC_f/SiC composite showed obvious non-linear characteristic curves, and the damage mainly occurred in the second, third, and fourth stages. The damage modes mainly included transverse matrix cracking, interlaminar cracking, longitudinal matrix cracking, and fiber bundle fracture.
(3) Matrix cracks tended to occur near the pores or holes of the material, and the number of longitudinal cracks was relatively high compared to the number of transverse cracks.
(4) It is recommended that preform of the composite can be optimized and denser composites will be preferable to improve their mechanical properties. Besides, numerical simulation can also be implemented to

verify the failure mechanisms concluding from the experiments.

Funding information: The work was supported by the National Natural Science Foundation of China (Grant No. 11802317) and the Project of Research Group on Advanced Textile Structural Composites (Grant No. QNTD202111).

Conflict of interest: Authors state no conflict of interest.

References

[1] Yajima S, Hayashi J, Omori M, Okamura K. Development of a silicon carbide fibre with high tensile strength. Nature. 1976;261:683–5.
[2] Yajima S, Hasegawa Y, Okamura K, Matsuzawa T. Development of high tensile strength silicon carbide fibre using an organosilicon polymer. Nature. 1978;273:525–7.
[3] Mungiguerra S, Cecere A, Savino R, Saraga F, Monteverde F, Sciti D. Improved aero-thermal resistance capabilities of ZrB_2-based ceramics in hypersonic environment for increasing SiC content. Corros Sci. 2021;178:109067.
[4] Croom BP, Xu P, Lahoda EJ, Deck CP, Li X. Quantifying the three-dimensional damage and stress redistribution mechanisms of braided SiC/SiC composites by *in situ* volumetric digital image correlation. Scr Mater. 2017;130:238–41.
[5] Arai Y, Aoki Y, Kagawa Y. Effect of cristobalite formation on the delamination resistance of an oxide/Si/(SiC/SiC) environmental barrier coating system after cyclic high temperature thermal exposure. Scr Mater. 2017;139:58–62.
[6] Baxevanakis C, Jeulin D, Renard J. Fracture statistics of a unidirectional composite. Int J Fract. 1995;73:149–81.
[7] Hui CY, Phoenix SL, Ibnabdeljalil M, Smith RL. An exact closed-form solution for fragmentation of Weibull fibers in a single filament composite with applications to fiber-reinforced ceramics. J Mech Phys Solids. 1995;43:1551–85.
[8] Lissart N, Lamon J. Damage and failure in ceramic matrix minicomposites: experimental study and model. Acta Mater. 1997;45:1025–44.
[9] DiBenedetto AT, Gurvich MR. Statistical simulation of fiber fragmentation in a single-fiber composite. Compos Sci Technol. 1997;57:543–55.
[10] Curtin WA, Ahn BK, Takeda N. Modeling brittle and tough stress–strain behavior in unidirectional ceramic matrix composites. Acta Mater. 1998;46:3409–20.
[11] Lamon J. Stochastic approach to multiple cracking in composite systems based on the extreme-values theory. Compos Sci Technol. 2009;69:1607–14.
[12] Castelier E, Gélébart L, Lacour C, Lantuéjoul C. Three consistent approaches of the multiple cracking process in 1D composites. Compos Sci Technol. 2010;70:2146–53.
[13] Phoenix SL. Statistical issues in the fracture of brittle-matrix fibrous composites. Compos Sci Technol. 1993;48:65–80.
[14] Bertrand S, Forio P, Pailler R, Lamon J. Hi-Nicalon/SiC minicomposites with (pyrocarbon/SiC)(n) nanoscale multilayered interphases. J Am Ceram Soc. 1999;82:2465–73.
[15] Martinez-Fernandez J, Morscher GN. Room and elevated temperature tensile properties of single tow Hi-Nicalon, carbon interphase, CVI SiC matrix minicomposites. J Eur Ceram Soc. 2000;20:2627–36.
[16] Stock SR. Recent advances in X-ray microtomography applied to materials. Int Mater Rev. 2008;53:129–81.
[17] Maire E, Withers PJ. Quantitative X-ray tomography. Int Mater Rev. 2014;59:1–43.
[18] Croom BP, Xu P, Lahoda EJ, Deck CP, Li X. Quantifying the three-dimensional damage and stress redistribution mechanisms of braided SiC/SiC composites by *in situ* volumetric digital image correlation. Scr Mater. 2017;130:238–41.
[19] Li T, Fan D, Lu L, Huang JY, Zhao JCE, Qi F, et al. Dynamic fracture of C/SiC composites under high strain-rate loading: microstructures and mechanisms. Carbon. 2015;91:468–78.
[20] Chateau C, Gelebart L, Bornert M, Crépin J, Boller E, Sauder C, et al. *In-situ* X-ray microtomography characterization of damage in SiC/SiC minicomposites. Compos Sci Technol. 2011;71:916–24.
[21] Zhang DX, Liu Y, Liu HL, Feng YQ, Guo HB, Hong ZL, et al. Characterisation of damage evolution in plain weave SiC/SiC composites using *in situ* X-ray micro-computed tomography. Compos Struct. 2021;275:114447.
[22] Ai SG, Song W, Chen YF. Stress field and damage evolution in C/SiC woven composites: image-based finite element analysis and *in situ* X-ray computed tomography tests. J Eur Ceram Soc. 2021;41:2323–34.
[23] Duan YD, Qiu HP, Yang TT, Wang L, Wang XM, Xie WJ, et al. Flexural failure mechanism of 2.5D woven SiC_f/SiC composites: combination of acoustic emission, digital image correlation and X-ray tomography. Compos Commun. 2021;28:100921.
[24] Mazars V, Caty O, Couégnat G, Bouterf A, Roux S, Denneulin S, et al. Damage investigation and modeling of 3D woven ceramic matrix composites from X-ray tomography *in-situ* tensile tests. Acta Mater. 2017;140:130–9.
[25] Yang HT, Xu SH, Zhang DX, Li LB, Huang XZ. *In-situ* tensile damage and fracture behavior of PIP SiC/SiC minicomposites at room temperature. J Eur Ceram Soc. 2021;41:6869–82.
[26] Quiney Z, Weston E, Nicholson PI, Pattison S, Bache MR. Volumetric assessment of fatigue damage in a SiC_f/SiC ceramic matrix composite via *in situ* X-ray computed tomography. J Eur Ceram Soc. 2020;40:3788–94.
[27] Gao, YT, Wang YD, Yang XM, Liu M, Xia, HH, Huai P, et al. Synchrotron X-ray tomographic characterization of CVI engineered 2D-woven and 3D-braided SiC_f/SiC composite. Ceram Int. 2016;42:17137–47.
[28] Gelebart L, Chateau C, Bornert M, Crepin J, Boller E. X-ray tomographic charaterization of the macroscopic porosity of chemical vapor infiltration SiCf/SiC composites: effects on the elastic behavior. Int J Appl Ceram Technol. 2010;7:348–60.